Fluorocarbon plasma etching and profile evolution of porous low-dielectric-constant silica

Arvind Sankaran[a] and Mark J. Kushner[b]
University of Illinois, 1406 West Green Street, Urbana, Illinois 61801

(Received 27 November 2002; accepted 27 January 2003)

To achieve shorter RC-delay times in integrated circuits low-dielectric-constant (low-k) materials are being investigated for interconnect wiring. Porous silicon dioxide (PS) is one such material. To address scaling issues during fluorocarbon plasma etching of PS, a feature profile model has been integrated with a plasma equipment model. To focus on issues related to the morphology of porous materials, the PS was treated as stoichiometric SiO_2. The model was validated by comparison to experiments for PS etching in CHF_3 plasmas sustained in an inductively coupled reactor. We found that etch rates (ER) for PS are generally higher than for SiO_2 due to the inherent smaller mass density, although ER do not necessarily scale linearly with pore size or porosity. Mass-corrected ER can be either larger or smaller than that of solid SiO_2. For example, in polymerizing environments, at high porosities and large pore radii, there is a reduction in ER due to pore filling with polymer. Profile scaling parameters, such as for tapering, observed for solid SiO_2, are generally applicable to PS. © *2003 American Institute of Physics.* [DOI: 10.1063/1.1562333]

As microelectronic device sizes continue to shrink, there is a propensity for increased delay in signal propagation in interconnect wiring due to higher resistances in the lines and larger capacitance between the lines.[1] Low-dielectric-constant (low-k) materials are being investigated as the insulators in interconnect wiring to reduce this delay. Low-k dielectrics can be broadly classified as organic and inorganic.[2] Organic materials, such as polytetrafluoroethylene and parylene, are etched in oxygen-based plasmas (O_2/Ar and O_2/N_2).[3,4] Inorganic dielectrics typically involve SiO_2-based materials etched in fluorocarbon plasmas.

Porous SiO_2 (PS) is one such inorganic low-k material. PS typically has average pore sizes of 2–20 nm and porosities of 20%–80%.[5,6] The dielectric constant is generally reduced in proportion to the mass density, which is inversely proportional to the porosity.[5,7] For example, Standaert *et al.* investigated fluorocarbon plasma etching of fluorinated SiO_2, hydrogen silsesquioxane, and methylsilsesquioxane, SiO_2-like films using an inductively coupled plasma and made comparisons to etching of conventional SiO_2 using a variety of fluorocarbon gases, including CHF_3.[7] The etch rates (ER) of PS were generally higher than that of conventional SiO_2 due to the lower mass densities of PS.

In this letter, the etching of PS will be discussed using results from a two-phase algorithm incorporated into the Monte-Carlo Feature Profile Model (MCFPM).[8,9] The MCFPM was integrated with the Hybrid Plasma Equipment Model, which provides the energy and angular distributions of the neutral and charged species incident on the wafer surface.[9,10] A surface reaction mechanism developed for fluorocarbon etching of SiO_2 similar to that discussed in Ref. 8 was applied to the investigation of etching of PS in CHF_3 plasmas. A schematic of the reaction mechanism is shown in Fig. 1. Etching of SiO_2 proceeds through the deposition of a fluorocarbon polymer overlayer.[11] C_xF_y radicals are the precursors to polymer deposition following ion activation of surface sites.[12] The polymer layer is consumed by energetic ion sputtering and F atom etching.[13] The polymer layer is the main inhibitor for the transport of species and delivery of activation energy to the SiO_2. As such, the ER generally scales inversely with the polymer thickness.[14] Upon delivery of activation energy to the polymer–SiO_2 interface, the oxygen in SiO_2 reacts with the fluorocarbon species in the polymer to release etch products, such as COF_x, thereby consuming the polymer.[15] Si in the SiO_2 reacts with F in the polymer to produce SiF_x products. A very thin polymer layer also produces low ER due to the lack of reactants in the overlying layer. Si is less reactive with the polymer, producing thicker films and lower ER for the same conditions.

Calibration and validation of the surface reaction mechanism was performed for three fluorocarbon gas chemistries; C_2F_6, C_4F_8, and CHF_3. The logic is that the reaction mechanism is an intrinsic property of the gas-phase reactant species and surface resident species, and thus should not depend on the source of gas phase fluxes. The choice of fluo-

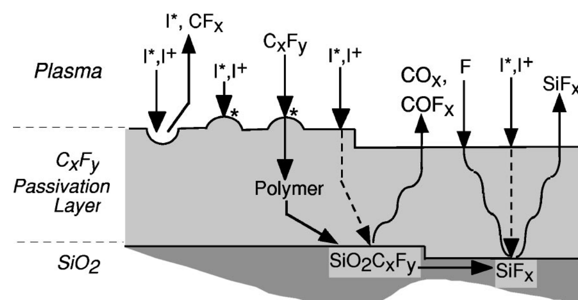

FIG. 1. Schematic of surface reaction mechanism for fluorocarbon etching of SiO_2/Si. I^+ refers to an ion. I* refers to a hot neutrals. The dashed lines represent energy transfer through the polymer. The curved lines represent species diffusion through the polymer.

[a]Department of Chemical Engineering; electronic mail: asankara@uiuc.edu
[b]Department of Electrical and Computer Engineering; electronic mail: mjk@uiuc.edu

0003-6951/2003/82(12)/1824/3/$20.00 © 2003 American Institute of Physics
Downloaded 21 Mar 2003 to 128.174.115.149. Redistribution subject to AIP license or copyright, see http://ojps.aip.org/aplo/aplcr.jsp

rocarbon plasma may determine the magnitudes and energies of the fluxes but the reaction mechanism should be the same. Comparisons of different fluorocarbon plasmas will be discussed elsewhere. For brevity, only CHF_3 plasma etching will be discussed here.

PS was modeled as stoichiometric SiO_2 with vacuum pores. The pore radii and locations were randomly chosen and distributed in the PS with a Gaussian distribution of radii having probability $p(r) \sim \exp\{-[(r-r_0)/\Delta r]^2\}$, where r is the radius of the pore incorporated, r_0 is the average pore radius, and Δr is the standard deviation. Algorithms were developed to distribute the pores so that the network of pores was independent, although we acknowledge that many varieties of PS have interconnected pores.

The etching reactor was an inductively coupled plasma (ICP) with a substrate bias, patterned after the apparatus used by Standaert *et al.*[5] The process conditions were 10 mTorr, 1400-W ICP power at 13.56 MHz and 50-sccm CHF_3. The substrate was biased at 3.4 MHz to vary the dc self-bias from 0 to 150 V. The CHF_3 reaction mechanism, based on Ref. 16, will be discussed elsewhere. Due to the high power densities, there is a large degree of dissociation of the CHF_3, and the smaller molecules have larger fluxes to the substrate. The resulting major polymerizing radicals are CF_2 and CF, and major ions are CF_3^+, CF_2^+, F^+, and H_2^+.

ER as a function of self-bias for PS (2-nm pores, 30% porosity; and 10-nm pores, 58% porosity) and solid SiO_2 compared to experiments[5] are shown in Fig. 2. At low biases and low ion energy, the polymer thickness is large (many nanometers) as there is insufficient ion energy to sputter the polymer, and ion-activated polymer deposition (which is largest at low energy) is rapid. The ER generally increase with increasing self-bias voltage as the incident ion energy increases. The onset of etching at a self-bias voltage of 40 eV for both solid SiO_2 and PS occurs as the polymer thins and energy is delivered through the polymer to the SiO_2 interface. At large biases the polymer thickness is submonolayer, and there is insufficient passivation to etch the SiO_2 layer, hence the ER saturates. The ER for the PS are higher than that of solid SiO_2 due to their inherent lower mass densities.

To isolate the effect of pores on ER, a corrected ER is defined as $C = \mathrm{ER} \cdot (1-p)$, where p is the porosity and ER is the gross etch rate. C is, effectively, the ER per unit mass. If pores had no kinetic effect on etching, C should be equal to the ER of solid SiO_2. Corrected ER as a function of self-bias are shown in Fig. 2(c). For 2-nm pores and 30% porosity, C exceeds the ER of solid SiO_2, which implies that the presence of small pores enhances the kinetic ER. In contrast, for 10-nm pores and 58% porosity, C is less than the ER of solid SiO_2, which implies that the presence of larger pores or higher porosity decreases the kinetic mass removal rate. Similar dependencies were obtained in experiments.[5]

In highly polymerizing etching environments, the steady state polymer thickness L can be many nanometers. As the PS is etched, pores are exposed and are filled with polymer. If $L \geqslant r_0$, as in the 2-nm case, then the increase in local polymer thickness due to pore filling is fractionally small compared to r_0. The end result should be that C is not significantly different from the ER of solid SiO_2. The increase of C above the ER of solid SiO_2 is likely due to a morphological effect related to the angle of incidence for optimum chemical sputtering. With the curvature of small open pores there are few surfaces without direct exposure to the plasma. However, compared to solid SiO_2, the average angle of incidence for ions to activate chemically enhanced sputtering is closer to the optimum at $\approx 60°$, so that activation of etch processes is likely more rapid.

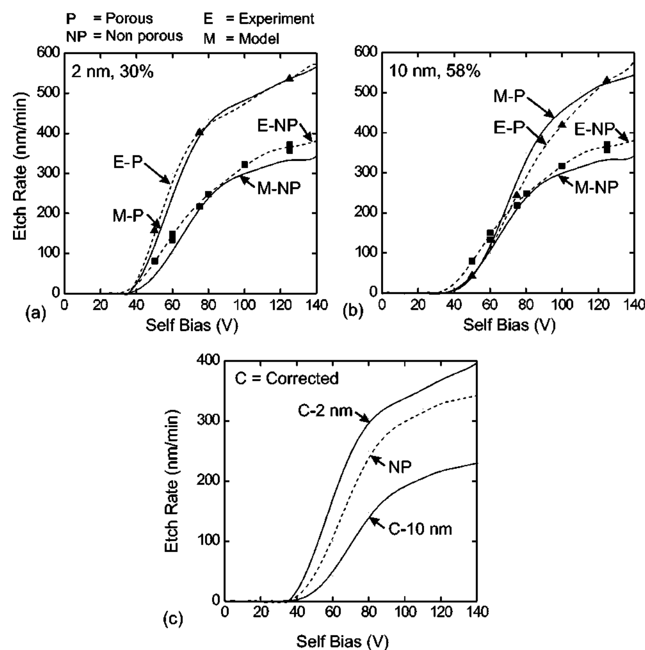

FIG. 2. Solid SiO_2 and PS ER as a function of self-bias voltage for a CHF_3 plasma for the base case conditions (a) PS having $r_0 = 2$-nm pores, 30% porosity, $\Delta r = 1.2$ nm, (b) $r_0 = 10$-nm pores, 58% porosity, $\Delta r = 5$ nm. (c) Corrected ER are enhanced by small pores and depressed by large pores. Experimental results are from Ref. 5 and are shown by the symbols.

If $L \leqslant r_0$, as for the 10-nm material, then as pores fill with polymer the thickness of the polymer can be significantly larger than L at local sites. This effect is more pronounced for bigger pores and larger porosities. The increased polymer layer thickness decreases delivery of activation energy to the SiO_2 interface and hence reduces the etch rates. The larger pores also have larger areas of SiO_2–polymer interfaces at shallow angles to the ion flux or which do not have line-of-sight to the ion flux. These locations must rely on reflected energetic particles for activation, fluxes which typically have lower energy. The end result is a lower ER per unit mass with C being less than the ER of solid SiO_2.

The consequences of pore filling were investigated for high-aspect-ratio (HAR) etching, (width of 0.1 μm, depth of ≈ 0.5 μm). Profiles for $r_0 = 2$ nm and 16 nm features are shown in Fig. 3. The Δr used for the 2-nm and 16-nm cases are 1.2 nm and 8 nm, respectively The polymer thickness is 5–10 nm, which is commensurate to or larger than the smaller pores, so that there is little variation in polymer thickness along the sidewalls or bottom of the trench. For the 16-nm material, as pores are exposed they fill with polymer, thereby increasing the effective polymer thickness. Such filling at the bottom of the feature slows the vertical ER, whereas on the sidewalls, the filling helps maintain the critical dimension by slowing lateral etching. Note that there are instances where pores are closed by either filling or lining with polymer. The jagged appearance of the profiles results

Downloaded 21 Mar 2003 to 128.174.115.149. Redistribution subject to AIP license or copyright, see http://ojps.aip.org/aplo/aplcr.jsp

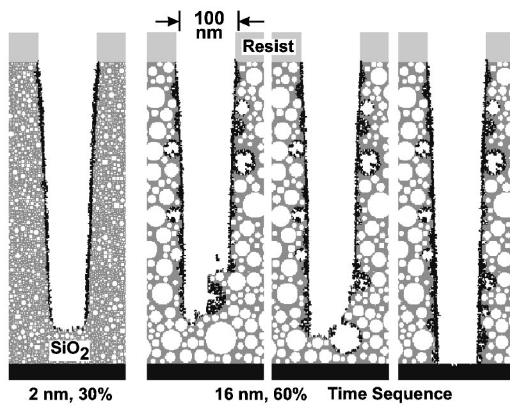

FIG. 3. Etch profiles for PS having $r_0 = 2$-nm pores, 30% porosity, $\Delta r = 1.2$ nm and $r_0 = 16$-nm pores with 60% porosity, $\Delta r = 8$ nm. The black shading represents polymer. Pore filling increases the effective polymer thickness for the larger pore material. A sequence of profiles is shown of the 16-nm material to demonstrate the pore breakthrough and filling process.

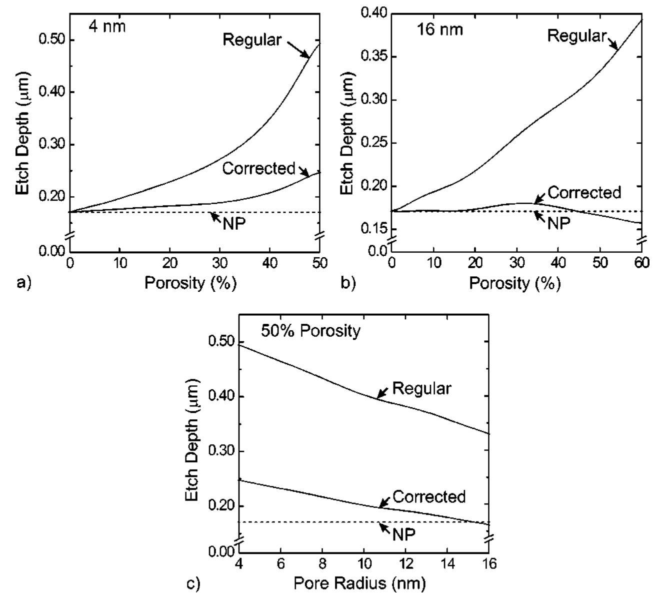

FIG. 4. Influence of porosity and pore radius on HAR features etched in a CHF_3 plasma. Trench depths are shown for equal etch times as a function of porosity for (a) $r_0 = 4$-nm pores, (b) $r_0 = 16$-nm pores, and (c) as a function of pore radius for 50% porosity. The Δr for all cases is 50% of the average pore radius.

from breakthrough of large, unfilled pores which advances the etch, and slow penetration through pores that are filled with polymer. Pore filling is problematic, as the polymer must later be removed, and the jagged surface sealed. The taper is not acutely sensitive to either pore radius or porosity, at least in a systematic manner. Scaling laws for tapering or bowing developed for solid SiO_2 are generally applicable to PS.

ER were examined for HAR trenches for a self-bias of 65 V, near threshold to emphasize these effects. The etch depth (after equal etch times) as a function of porosity (for $r_0 = 4$-nm and 16-nm pores) and pore radius (for 50% porosity) are shown in Fig. 4. The Δr for all cases is 50% of the average pore radius. In agreement with earlier observations, the smaller 4-nm pores enhance the rates for HAR etching compared to solid SiO_2. The enhancement increases with porosity as the more favorable angle of incidence is more widely distributed. In contrast, the 16-nm pores have at best a neutral effect and at worst moderately decrease the mass removal rate. This is in contrast to blanket etching where, for similar conditions, C is significantly below the ER of solid SiO_2. The increase in ER, if any, decreases with increasing pore size, as shown in Fig. 4(c) for a porosity of 50%. The ER, gross and corrected, decrease with increasing pore size, as pore filling becomes more important with $L \leqslant r_0$.

In conclusion, the etching of PS has been investigated using a two-phase feature profile model. The ER of PS were higher than that of solid SiO_2 due to inherent lower mass densities. Mass-corrected ER may exceed or be less than the ER of solid SiO_2 dependent on the character of pore filling by polymers. When $L \geqslant r_0$ smaller pores enhance the ER due to more optimal angel of incidence of ion fluxes for chemical sputtering. When $L \leqslant r_0$ for larger pores with high porosity, the effective polymer thickness is larger. The resulting lower rate of ion activation, less favorable angles of incidence of the ion flux and ion shadowing reduces the rate of mass removal.

This work was supported by the National Science Foundation (CTS99-74962), Semiconductor Research Corp., and SEMATECH.

[1] S.-J. Wang, H.-H. Park, and G.-Y. Yeom, Jpn. J. Appl. Phys. **39**, 7007 (2000).
[2] G. S. Oehrlein, T. E. F. M. Standaert, and P. J. Matsuo, in *Solid State Technology*, (...,...2000), p. 125.
[3] T. E. F. M. Standaert, P. J. Matsuo, X. Li, G. S. Oehrlein, T. M. Lu, R. Gutmann, C. T. Rosenmayer, J. W. Bartz, J. G. Langan, and W. R. Entley, J. Vac. Sci. Technol. A **19**, 435 (2001).
[4] D. Fuard, O. Joubert, L. Vallier, and M. Bonvalot, J. Vac. Sci. Technol. B **19**, 447 (2001).
[5] T. E. F. M. Standaert, E. A. Joseph, G. S. Oehrlein, A. Jain, W. N. Gill, P. C. J. Wayner, and J. L. Plawsky, J. Vac. Sci. Technol. A **18**, 2742 (2000).
[6] S. V. Nitta, V. Pisupatti, A. Jain, J. Wayner, P. C. , W. N. Gill, and J. L. Plawsky, J. Vac. Sci. Technol. B **17**, 205 (1999).
[7] T. E. F. M. Standaert, P. J. Matsuo, S. D. Allen, G. S. Oehrlein, and T. J. Dalton, J. Vac. Sci. Technol. A **17**, 741 (1999).
[8] D. Zhang and M. J. Kushner, J. Vac. Sci. Technol. A **19**, 524 (2001).
[9] J. Lu and M. J. Kushner, J. Vac. Sci. Technol. A **19**, 2652 (2001).
[10] R. L. Kinder and M. J. Kushner, J. Appl. Phys. **90**, 3699 (2001).
[11] A. J. Bariya, C. W. Frank, and J. P. McVittie, J. Electrochem. Soc. **137**, 2575 (1990).
[12] T. E. F. M. Standaert, M. Schaepkens, N. R. Rueger, P. G. M. Sebel, G. S. Oehrlein, and J. M. Cook, J. Vac. Sci. Technol. A **16**, 239 (1998).
[13] K. Miyata, M. Hori, and T. Goto, J. Vac. Sci. Technol. A **14**, 2083 (1996).
[14] N. R. Rueger, J. J. Beulens, M. Schaepkens, M. F. Doemling, J. M. Mirza, T. E. F. M. Standaert, and G. S. Oehrlein, J. Vac. Sci. Technol. A **15**, 1881 (1997).
[15] M. Matsui, T. Tatsumi, and M. Sekine, J. Vac. Sci. Technol. A **19**, 2089 (2001).
[16] M. J. Kushner and D. Zhang, J. Appl. Phys. **88**, 3231 (2000).

Downloaded 21 Mar 2003 to 128.174.115.149. Redistribution subject to AIP license or copyright, see http://ojps.aip.org/aplo/aplcr.jsp